Adsorption 8: 171–188, 2002

A Branched Pore Model Analysis for the Adsorption of Acid Dyes on Activated Carbon

DANNY C.K. KO, JOHN F. PORTER AND GORDON McKAY*
Department of Chemical Engineering, Hong Kong University of Science and Technology, Clear Water Bay, Kowloon, Hong Kong SAR, Peoples' Republic of China
kemckayg@ust.hk

Received September 5, 2001; Revised May 16, 2002; Accepted July 10, 2002

Abstract. A new branched-pore adsorption model has been developed using an external mass transfer coefficient, K_f, an effective diffusivity, D_{eff}, a lumped micropore diffusion rate parameter, K_b, and the fraction of macropores, f, to describe sorption kinetic data from initial adsorbent-adsorbate contact to the long-term adsorption phase. This model has been applied to an environmental pollution problem—the removal of two dyes, Acid Blue 80 (AB80) and Acid Red 114 (AR114), by sorption on activated carbon. A computer program has been used to generate theoretical concentration-time curves and the four mass transfer kinetic parameters adjusted so that the model achieves a close fit to the experimental data. The best fit values of the parameters have been determined for different initial dye concentrations and carbon masses. Since the model is specifically applicable to fixed constant values of these four parameters, a further and key application of this project is to see if single constant values of these parameters can be used to describe all the experimental concentration-time decay curves for one dye-carbon system.

The error analysis and best fit approach to modeling the decay curves for both dye systems show that the correlation between experimental and theoretical data is good for the fixed values of the four fitted parameters. A significantly better fit of the model predictions is obtained when K_f, K_b and f are maintained constant but D_{eff} is varied. This indicates that the surface diffusivity may vary as a function of surface coverage.

Keywords: adsorption model, acid dye, activated carbon, macropore, micropore, variable surface diffusivity

Introduction

Adsorption with significant mass transfer resistance is commonly described by four models. Three of these models use different representations of diffusion within the porous adsorbent particle, while the fourth is based on sorption reaction kinetics (Yiacoumi and Tien, 1995). The adsorption reaction is assumed rapid with respect to the other rate processes in the majority of the models.

Wild developed a diffusion model using linear driving force expressions for external and internal transport processes (Wild, 1980). When the adsorption isotherm is linear, analytical solutions are available. However, the particle mass transfer coefficient varies with the particle diameter in both this model and the reaction rate model. Keinath and Weber (1968) reported that, for dinitro-o-sec-butyl phenol, the intraparticle mass transfer coefficient, k, varies with the initial concentration and with $d_p^{-1.4}$, where d_p is the diameter of the particle. Griffin and Dranoff (1963) reported that for glycerol adsorption on ion-exchange resins, k, varies with $d_p^{-1.6}$. From theoretical considerations, Glueckauf (1955) and Jury (1967) have shown that k should vary with d_p^{-2} for $D_s t/R^2 > 0.1$, where D_s is the internal surface diffusion coefficient, R is the particle radius and t is the time. The condition $D_s t/R^2 > 0.1$ can only be satisfied in most cases for small particles, large internal

*Author to whom all correspondence should be addressed.

diffusion coefficients, or large time values. Negligible intraparticle diffusion resistance or rapid approach to equilibrium is implied by the former two cases and the third condition is only reached when the particle is near equilibrium and the concentration profile in the particle is nearly flat.

For the determination of batch adsorption rates of single organic solutes, an analytical solution has been obtained, assuming external mass transfer, pore diffusion and irreversible adsorption (Spahn and Schlunder, 1975). In the pore phase diffusion model, the adsorbent particle is seen as consisting of a solid phase interspersed with very small pores where the adsorbate diffuses into the pores in the fluid phase and adsorption occurs at the internal surfaces. Kasten and Amundson (1952), and Edeskuty and Amundson (1952), obtained analytical solutions in terms of infinite series for linear adsorption isotherms with fixed bed and batch reactors. DiGiano and Weber (1972) studied adsorption in finite and infinite bath systems by using the same approach. Assumptions of irreversible immobilization and quasi-steady state in the solid phase were made in the finite bath system. Other applications based on parabolic concentration profiles within the particle have been studied by Tien (1994) and the effects of the energy distribution profile in branched pore models for gas adsorption have been studied by Do (1998), Hu (1999), and Hu et al. (1999).

Mathews and Weber (1976) developed a solid-phase diffusion model using finite difference approximations for any arbitrary isotherm and extended the model to multicomponent systems. They also verified it for a wide range of binary mixtures. Successful application of this approach to several solutes and mixtures in batch reactors and fixed-beds has now been achieved (Crittenden and Weber, 1978a, 1978b; Lee et al., 1980; Weber and Liu, 1980; Thacker et al., 1981; McKay, 1984a).

Dedrick and Beckmann (1967) compared pore phase and solid phase diffusion models using a series of batch experiments. An irreversible isotherm assumption was made for the pore phase model, even though it was found that the experimental isotherm was described by the Freundlich equation. Both models were seen to fit the data equally well. Batch studies were conducted by Hsieh et al. (1969) to correlate diffusional data based on both models and they found less scatter with the solid phase diffusion model. Weber and Chakravorti (1974) also compared the two models, concluding that for solutes with non-linear isotherms, batch or fixed-bed experiments must be carried out with the solute under consideration and compared with both model predictions before a model can be selected.

Other models of greater complexity have been proposed. Neretnieks (1976) modeled diffusion rates using a concentration dependent diffusion coefficient. Famularo et al. (1980), Peel et al. (1981), and Weber and Liang (1983) proposed models, which take into account the distribution of macropores and micropores in activated carbon. Activated carbon is the most widely used adsorbent in wastewater treatment (Allen et al., 1992). In this work, activated carbon has been used to remove two dyes, Acid Blue 80 and Acid Red 114 from aqueous solution.

A branched-pore kinetic model (BPKM), based on external mass transfer, a fraction, f, of the total adsorption capacity termed macropores and a fraction, $1 - f$, to the micropores, has been used to predict the performance of a batch adsorber. A computer program has been developed to generate theoretical concentration-time curves based on this model and the mass transfer parameters adjusted to maximize the correlation with experimentally measured concentration-time decay curves by a "best fit"approach. A sensitivity analysis has also been performed to study the effect of the four mass-transfer parameters of the model—external mass transfer coefficient K_f, effective diffusivity D_{eff}, lumped micropore diffusion rate parameter K_b and f is a fraction of the total adsorption capacity allocated to "macropores"—on the shape of the concentration decay curves. The variables of initial dye concentration and carbon mass have been successfully correlated using constant values of the mass-transfer parameters K_f, K_b and f, and the effective diffusivity D_{eff} shows a linear function of fractional surface coverage.

Model Description

Previous analyses on the single and two-resistance mass transfer models (McKay, 1984b) show that these models agree with experimental results but only over very limited regions of the adsorption period—indicating that another internal mass transfer resistance becomes rate controlling at long time periods. A computer model similar to that presented by Peel et al. (1981) has been developed, incorporating three mass transfer resistances and dividing the adsorbent particle into two regions of different diffusion rates. These two regions are loosely termed 'macropores' and 'micropores'—relatively rapid diffusion and

adsorption occurs in the macropores and the remaining slow approach to equilibrium occurs in the micropores. The three mass transfer resistances are:

1. Diffusion of solute from solution, across the external liquid boundary layer onto the adsorbent surfaces.
2. Diffusion onto and adsorbing in the macropore region.
3. Diffusion onto and adsorbing in the micropore region.

To describe transport into the micropores, a lumped parameter approach has been used. The particle is partitioned into two regions: a fraction f of the total adsorption capacity to macropores; a fraction, $(1-f)$, constituting the micropores. Transport between the two regions, which are both distributed radially, is described by a linear driving force expression between the local macro- and micropore concentrations.

The present solution method is based on solving the four key transport controlling equations using a Crank-Nicolson finite difference approach (Crank and Nicolson, 1947) combined with banded matrix techniques (NAG, 1993).

Mathematical Development

Equilibrium as described by the equilibrium isotherms holds at the interface between the liquid and solid phases. In this case the model uses the Langmuir isotherm

$$q_s = \frac{K_L C_s}{1 + a_L C_s} \tag{1}$$

The mass balance equations for the various sections of the system can be written as follows:

1. Liquid-phase mass balance.

$$V\frac{dC_t}{dt} = -K_f A(C_t - C_{s,t}) \tag{2}$$

2. Macropore mass balance. If the fraction f represents that part of the total adsorptive capacity utilized in the macropore region, the balance can be written:

$$f\frac{\partial q_m}{\partial t} = \frac{f D_{\text{eff}}}{r^2}\frac{\partial}{\partial r}\left(r^2\frac{\partial q_m}{\partial r}\right) - R_b \tag{3}$$

   The introduction of this fraction is equivalent to dividing the adsorbent volume and mass into two homogeneously distributed regions. R_b is the rate of transfer of adsorbate from the macropore network to the micropores or branch pores.
3. Micropore mass balance.

$$(1-f)\frac{\partial q_b}{\partial t} = K_b(q_m - q_b) = R_b \tag{4}$$

In addition, the following initial and boundary conditions apply:

$$q_m(r, 0) = 0 \tag{5}$$

$$q_b(r, 0) = 0 \tag{6}$$

$$C_t(t = 0) = C_0 \tag{7}$$

$$q_m(R, t) = q_s(t) \tag{8}$$

$$\frac{\partial q_m}{\partial r}(0, t) = 0 \tag{9}$$

In previous models (Peel et al., 1981; McKay et al., 1987), the coupling between the liquid and solid phases was achieved by equating the fluxes at the solid-liquid interface:

$$K_f A(C_t - C_{s,t}) = f D_{\text{eff}} A\rho\left(\frac{\partial q_m}{\partial r}\right)_{r=R} \tag{10}$$

Equation (10) ignores the contribution from the micropore fraction of the adsorbent, therefore in the present model Eq. (11) has been used:

$$f\frac{\partial q_m}{\partial t} + (1-f)\frac{\partial q_b}{\partial t} = \frac{f D_{\text{eff}}}{r^2}\frac{\partial}{\partial r}\left(r^2\frac{\partial q_m}{\partial r}\right) = \frac{k_f A}{\rho V}(C - C_s) \tag{11}$$

Equations (2)–(4) and (11) are first reduced to dimensionless form using the substitutions:

$$C = \frac{C_t}{C_0}, \quad C_s = \frac{C_{s,t}}{C_0}, \quad Q = \frac{q}{q_0}, \tag{12}$$

$$\beta = \frac{r}{R}, \quad \text{and} \quad \theta = \frac{(D_{\text{eff}} t)}{R^2} \tag{13}$$

The change variable:

$$\eta = \beta^2 \tag{14}$$

is introduced to give a finer spatial grid near the surface of the particle where concentration gradients are highest.

The resultant set of equations is:

$$\frac{\partial Q_m}{\partial \theta} = 4\eta \frac{\partial^2 Q_m}{\partial \eta^2} + 4\frac{\partial Q_m}{\partial \eta} - \frac{1-f}{f}\frac{\partial Q_b}{\partial \theta} \tag{15}$$

$$\frac{\partial Q_b}{\partial \theta} = PBiot\frac{f}{1-f}(Q_m - Q_b) \tag{16}$$

$$\frac{\partial C}{\partial \theta} = -3f \cdot \frac{FBiot}{SFact}(C - C_s) \tag{17}$$

$$\left(\frac{\partial Q_m}{\partial \eta}\right)_{\eta=1} = \left(\frac{FBiot}{2}\right)(C - C_s) \tag{18}$$

In previous papers (Peel et al., 1981, McKay et al., 1987), the authors used 4, 6, 1 as the coefficients for the right hand side of Eq. (15). Yang and Al-Duri (2001) did not state the resultant set of equations. However, the following equations confirm that the coefficients should be 4, 4, 1.

$$\begin{aligned} f\frac{\partial q_m}{\partial t} &= \frac{f D_{\text{eff}}}{r^2}\frac{\partial}{\partial r}\left(r^2\frac{\partial q_m}{\partial r}\right) - (1-f)\frac{\partial q_b}{\partial t} \\ &= \frac{f D_{\text{eff}}}{r^2}\left(r^2\frac{\partial^2 q_m}{\partial r^2} + 2r\frac{\partial q_m}{\partial r}\right) - (1-f)\frac{\partial q_b}{\partial t} \end{aligned} \tag{19}$$

$$\begin{aligned} & f\frac{q_0 \cdot \partial Q_m}{\left(\frac{R^2}{D_{\text{eff}}} \cdot \partial\theta\right)} \\ &= \frac{f D_{\text{eff}}}{r^2}\left(r^2\frac{q_0 \cdot \partial^2 Q_m}{\left(\frac{R^2}{2r} \cdot \partial\eta\right)^2} + 2r\frac{q_0 \cdot \partial Q_m}{\left(\frac{R^2}{2r} \cdot \partial\eta\right)}\right) \\ &\quad - (1-f)\frac{q_0 \cdot \partial Q_b}{\left(\frac{R^2}{D_{\text{eff}}} \cdot \partial\theta\right)} \end{aligned} \tag{20}$$

Rearranging,

$$\begin{aligned} f\frac{D_{\text{eff}}}{R^2}\frac{q_0 \cdot \partial Q_m}{\partial \theta} &= \frac{f \cdot D_{\text{eff}}}{r^2}\left(r^2 \cdot \frac{4 \cdot r^2}{R^4} \cdot \frac{q_0 \cdot \partial^2 Q_m}{\partial \eta^2}\right. \\ &\quad \left. + 2r \cdot \frac{2r}{R^2} \cdot \frac{q_0 \cdot \partial Q_m}{\partial \eta}\right) \\ &\quad - (1-f)\frac{D_{\text{eff}}}{R^2}\frac{q_0 \cdot \partial Q_b}{\partial \theta} \end{aligned} \tag{21}$$

Simplifying by q_0 and D_{eff}:

$$\begin{aligned} f\frac{1}{R^2}\frac{\partial Q_m}{\partial \theta} &= \frac{f}{r^2}\left(\frac{4 \cdot r^4}{R^4} \cdot \frac{\partial^2 Q_m}{\partial \eta^2} + \frac{4r^2}{R^2} \cdot \frac{\partial Q_m}{\partial \eta}\right) \\ &\quad - (1-f)\frac{1}{R^2}\frac{\partial Q_b}{\partial \theta} \end{aligned} \tag{22}$$

Dividing the two sides by f/R^2 and simplifying:

$$\begin{aligned} \frac{\partial Q_m}{\partial \theta} &= \frac{R^2}{r^2}\left(\frac{4 \cdot r^4}{R^4} \cdot \frac{\partial^2 Q_m}{\partial \eta^2} + \frac{4r^2}{R^2} \cdot \frac{\partial Q_m}{\partial \eta}\right) \\ &\quad - \frac{1-f}{f} \cdot \frac{\partial Q_b}{\partial \theta} \\ &= \frac{4 \cdot r^2}{R^2} \cdot \frac{\partial^2 Q_m}{\partial \eta^2} + 4 \cdot \frac{\partial Q_m}{\partial \eta} - \frac{1-f}{f} \cdot \frac{\partial Q_b}{\partial \theta} \end{aligned} \tag{23}$$

Finally

$$\frac{\partial Q_m}{\partial \theta} = 4\eta \frac{\partial^2 Q_m}{\partial \eta^2} + 4\frac{\partial Q_m}{\partial \eta} - \frac{(1-f)}{f}\frac{\partial Q_b}{\partial \theta} \tag{15}$$

Equations (15)–(18) are the transformed equations for macropore and micropore mass balance equations, the coupling equation and liquid phase mass balance equation respectively where

$$FBiot = \frac{K_f C_0 R}{\rho f D_{\text{eff}} q_0} \tag{24}$$

$$PBiot = \frac{K_b R^2}{f D_{\text{eff}}} \tag{25}$$

$$SFact = \frac{V C_0}{m q_0} \tag{26}$$

The initial and boundary conditions (5)–(9) become

$$Q_m(\eta, 0) = 0 \tag{27}$$

$$Q_b(\eta, 0) = 0 \tag{28}$$

$$C(0) = 1 \tag{29}$$

$$Q_m(1, t) = Q_s(t) \tag{30}$$

The set of Eqs. (15)–(18) is solved using Crank-Nicolson finite difference techniques. To avoid multiple subscripts, Q_m is replaced by Q and Q_b by $\bar{Q}$. Making those substitutions and rearranging Eq. (15) for integration, we obtain

$$\begin{aligned} & \int_\theta^{\theta+\Delta\theta} \frac{\partial Q}{\partial \theta} + \frac{1-f}{f}\frac{\partial \bar{Q}}{\partial \theta}\, d\theta \\ &= \int_\theta^{\theta+\Delta\theta} 4\eta\frac{\partial^2 Q}{\partial \eta^2} + 4\frac{\partial Q}{\partial \eta}\, d\theta \end{aligned} \tag{31}$$

$$\begin{aligned} & \left(Q + \frac{1-f}{f}\bar{Q}\right)(\theta + \Delta\theta) - \left(Q + \frac{1-f}{f}\bar{Q}\right)\theta \\ &= \int_\theta^{\theta+\Delta\theta} 4\eta\frac{\partial^2 Q}{\partial \eta^2} + 4\frac{\partial Q}{\partial \eta}\, d\theta \end{aligned} \tag{32}$$

The boundary condition stated in Eq. (9) is satisfied implicitly through the choice of the substitution variable η.

We introduce finite difference meshes of spacing $\Delta\eta$ and $\Delta\theta$ in the spatial and time variables η and θ respectively. The grid points of the η mesh are labeled by p and those of the θ mesh by n.

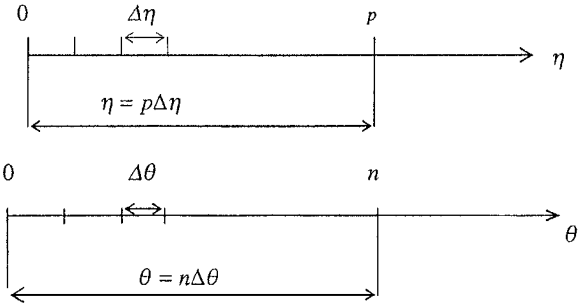

Using a space mesh and a time mesh as illustrated above, Eq. (32) becomes

$$\left(Q_p^{n+1} - Q_p^n\right) + \frac{1-f}{f}\left(\bar{Q}_p^{n+1} - \bar{Q}_p^n\right) = \int_{n\Delta\theta}^{(n+1)\Delta\theta} 4\eta\frac{\partial^2 Q}{\partial\eta^2} + 4\frac{\partial Q}{\partial\eta}\,d\theta \tag{33}$$

where Q_p^n is the value of Q at the pth mesh point in $\eta(=p\Delta\eta)$ and the nth mesh point in $\theta(=n\Delta\theta)$.

The right hand side can be approximated by using the trapezium rule

$$\text{R.H.S.} = \frac{\Delta\theta}{2}\left|\left\{4\eta\frac{\partial^2 Q}{\partial\eta^2} + 4\frac{\partial Q}{\partial\eta}\right\}^{n+1} + \left\{4\eta\frac{\partial^2 Q}{\partial\eta^2} + 4\frac{\partial Q}{\partial\eta}\right\}^{n}\right| \tag{34}$$

Using the central difference formulae

$$\frac{\partial Q}{\partial\eta} = \frac{Q_{p+1}^n - Q_{p-1}^n}{2\Delta\eta} \tag{35}$$

and

$$\frac{\partial^2 Q}{\partial\eta^2} = \frac{Q_{p+1}^n - 2Q_p^n + Q_{p-1}^n}{(\Delta\eta)^2} \tag{36}$$

Equation (34) becomes

$$\text{R.H.S.} = \frac{\Delta\theta}{2}\left|4p\Delta\eta\left(\frac{Q_{p+1}^{n+1} - 2Q_p^{n+1} + Q_{p-1}^{n+1}}{(\Delta\eta)^2}\right) + 4\left(\frac{Q_{p+1}^{n+1} - Q_{p-1}^{n+1}}{2\Delta\eta}\right) + 4p\Delta\eta\left(\frac{Q_{p+1}^{n} - 2Q_p^{n} + Q_{p-1}^{n}}{(\Delta\eta)^2}\right) + 4\left(\frac{Q_{p+1}^{n} - Q_{p-1}^{n}}{2\Delta\eta}\right)\right| \tag{37}$$

Substituting Eq. (37) into Eq. (33), introducing $S_1 = \Delta\theta/\Delta\eta$ and rearranging, we obtain

$$\begin{aligned} &-S_1(2p+1)Q_{p+1}^{n+1} + (1+4pS_1)Q_p^{n+1} \\ &- S_1(2p-1)Q_{p-1}^{n+1} + \left(\frac{1-f}{f}\right)\bar{Q}_p^{n+1} \\ &= S_1(2p+1)Q_{p+1}^{n} + (1-4pS_1)Q_p^{n} \\ &+ S_1(2p-1)Q_{p-1}^{n} + \left(\frac{1-f}{f}\right)\bar{Q}_p^{n} \\ &\qquad \text{for } 1 \le p \le M-1 \end{aligned} \tag{38}$$

Equation (16) states

$$\frac{\partial\bar{Q}}{\partial\theta} = PBiot\frac{f}{1-f}(Q - \bar{Q})$$

Integrating the above equation

$$\int_{\theta}^{\theta+\Delta\theta}\frac{\partial\bar{Q}}{\partial\theta}\,d\theta = PBiot\frac{f}{1-f}\int_{\theta}^{\theta+\Delta\theta}(Q-\bar{Q})\,d\theta \tag{39}$$

The R.H.S. reduces to

$$\text{R.H.S.} = PBiot\frac{f}{1-f}\left[\frac{\Delta\theta}{2}(Q-\bar{Q})_{\theta+\Delta\theta} + (Q-\bar{Q})_{\theta}\right] = \frac{PBiot\cdot f}{1-f}\cdot\frac{\Delta\theta}{2}[Q_{\theta+\Delta\theta} - \bar{Q}_{\theta+\Delta\theta} + Q_{\theta} - \bar{Q}_{\theta}]$$

reverting to the p-n notation

$$\bar{Q}_p^{n+1} - \bar{Q}_p^n = PBiot\frac{f}{1-f}\frac{\Delta\theta}{2}\left(Q_p^{n+1} + Q_p^n - \bar{Q}_p^{n+1} - \bar{Q}_p^n\right) \tag{40}$$

Introducing a constant S_2 such that

$$S_2 = PBiot\frac{f\,\Delta\theta}{2(1-f)} \tag{41}$$

Then

$$\bar{Q}_p^{n+1} - \bar{Q}_p^n = S_2\left(Q_p^{n+1} + Q_p^n - \bar{Q}_p^{n+1} - \bar{Q}_p^n\right) \tag{42}$$

Rearranging:

$$\bar{Q}_p^{n+1} + S_2\bar{Q}_p^{n+1} - S_2Q_p^{n+1} = S_2Q_p^n - S_2\bar{Q}_p^n + \bar{Q}_p^n \tag{43}$$

$$(1+S_2)\bar{Q}_p^{n+1} - S_2 Q_p^{n+1} = (1-S_2)\bar{Q}_p^n + S_2 Q_p^n \quad \text{for } 0 \le p \le M \quad (44)$$

At the centre of the particle, Eq. (15) reduces to

$$\frac{\partial Q}{\partial \theta} = 4\frac{\partial Q}{\partial \eta} - PBiot(Q-\bar{Q}) = 4\frac{\partial Q}{\partial \eta} - \frac{1-f}{f}\frac{\partial \bar{Q}}{\partial \theta} \quad (45)$$

Using a forward-difference approximation and integrating the above with respect to θ

$$Q_0^{n+1} - Q_0^n + \frac{1-f}{f}\left(\bar{Q}_0^{n+1} - \bar{Q}_0^n\right) = \frac{4\Delta\theta}{2}\left[\left(\frac{\partial Q}{\partial \eta}\right)^{n+1} + \left(\frac{\partial Q}{\partial \eta}\right)^{n}\right] = 2\Delta\theta\left\{\frac{Q_1^{n+1} - Q_0^{n+1}}{\Delta\eta} + \frac{Q_1^n - Q_0^n}{\Delta\eta}\right\} \quad (46)$$

or

$$Q_M^{n+1} - Q_{M-1}^{n+1} = S_4\left(C^{n+1} - C_s^{n+1}\right) \quad (49)$$

where

$$S_4 = \frac{\Delta\eta}{2} FBiot \quad (50)$$

The liquid phase mass balance Eq. (17) becomes

$$C^{n+1} = \frac{(1-S_3)C^n + S_3\left(C_s^n + C_s^{n+1}\right)}{(1+S_3)} \quad (51)$$

where

$$S_3 = \frac{3f(FBiot)\Delta\theta}{2SFact} \quad (52)$$

The set of Eqs. (38), (44), (47), (49) and (51) can be conveniently written in matrix form as shown below.

The Solution Matrix

$$\begin{array}{c} \underline{\text{ROW}} \\ 1 \\ 2 \\ 3 \\ 4 \\ 5 \\ . \\ . \\ 2M-1 \\ 2M \\ 2M+1 \\ 2M+2 \end{array} \begin{bmatrix} 1+2s_1 & (1-f)/f & -2S_1 & 0 & 0 & 0 & 0 \\ -S_2 & 1+S_2 & 0 & 0 & 0 & 0 & 0 \\ -S_1 & 0 & 1+4S_1 & (1-f)/f & -3S_1 & 0 & 0 \\ 0 & 0 & -S_2 & 1+S_2 & 0 & 0 & 0 \\ 0 & 0 & -3S_1 & 0 & 1+8S_1 & (1-f)/f & -5S_1 \\ & & & & & & \\ & & & & & & \\ & & & & & & \\ & & & & & & \\ -1 & 0 & 1 & 0 & & & \\ 0 & 0 & -S_2 & 1+S_2 & & & \end{bmatrix} \begin{bmatrix} \underline{\text{Q}} \\ Q_0^{n+1} \\ \bar{Q}_0^{n+1} \\ Q_1^{n+1} \\ \bar{Q}_1^{n+1} \\ Q_2^{n+1} \\ . \\ . \\ . \\ . \\ Q_m^{n+1} \\ \bar{Q}_m^{n+1} \end{bmatrix} = \begin{bmatrix} \underline{\text{Z}} \\ Z_0 \\ \bar{Z}_0 \\ Z_1 \\ \bar{Z}_1 \\ Z_2 \\ . \\ . \\ . \\ . \\ Z_m \\ \bar{Z}_m \end{bmatrix}$$

Rearranging Eq. (46) and substituting S_1 for $\Delta\theta/\Delta\eta$ gives

$$(1+2S_1)Q_0^{n+1} + \left(\frac{1-f}{f}\right)\bar{Q}_0^{n+1} - 2S_1 Q_1^{n+1} = (1-2S_1)Q_0^n + \left(\frac{1-f}{f}\right)\bar{Q}_0^n + 2S_1 Q_1^n \quad (47)$$

The boundary condition Eq. (18) becomes

$$Q_M^{n+1} - Q_{M-1}^{n+1} = \frac{\Delta\eta}{2} FBiot\left(C^{n+1} - C_s^{n+1}\right) \quad (48)$$

The column vector Q on the LHS of the matrix contains alternating values of Q_p^{n+1} and $\bar{Q}_p^{n+1}$. The first row of matrix A derives from Eq. (47), the odd numbered rows $p=3$ to $p=2M-1$ come from (38), the even numbered rows are from (44) and row $(2M+1)$ comes from (49). The resultant matrix is diagonally banded with a bandwidth of five elements. Z_p is equal to RHS of (47) for $p=0$, to the RHS of (38) for $1 \le p \le M-1$ and to the RHS of (49) for $p=M$, $\bar{Z}_p$ is the RHS of (44). Note the rows are numbered from 1 to $2M+2$ corresponding to $p=0$ to $p=M$.

Once Z_p and $\bar{Z}_p$ are known, the $\underline{\underline{A}}$ matrix may be inverted to yield the values of Q and $\bar{Q}$ at time $(n+1)$. Knowing these values, C_s^{n+1} can be calculated from (1) and hence C^{n+1} form (51). A slight difficulty occurs at this stage due to the fact that Z_p, for $p = 0$ to $(M-1)$ and $\bar{Z}_p$, for $p=0$ to M, are expressed in terms of equalities at time n, so Z_m requires knowledge of $(C^{n+1}-C_s^{n+1})$ at time $(n+1)$. To overcome this problem, the approach adopted is to estimate $(C^{n+1}-C_s^{n+1})$ from the results at time n and then follow an interation procedure until the estimate of $(C^{n+1}-C_s^{n+1})$ is in agreement with the values calculated from (1) and (51) using the Q^{n+1} obtained from the matrix solution.

Experimental Techniques

Adsorbent

The adsorbent used in this investigation was activated carbon type F400 provided from Filtrasorb Corporation. It was sieved in the laboratory to obtain a discrete size range of 500–710 microns and dried at a 110°C in an oven for 24 hours. Although the particles appeared irregularly shaped under a microscope, they approximated more closely to spheres than to cylinders or parallel pipes for the size range under investigation. Thus they were assumed to be spheres having a diameter given by the arithmetic mean value between respective mesh sizes, that is 605 microns.

Adsorbates

The adsorbates used in the experiments are listed below. The dyestuffs were used as the commercial salts.

1. Acid Red 114 was supplied by Sigma-Aldich Chemical Company.
2. Acid Blue 80 was supplied by Ciba Specialty Chemicals.

Preparation of Calibration Curve

The dyes were made up in stock solutions of concentration 1000 ppm and were subsequently diluted to the required concentrations with deionised water. Calibration curves for each dye were prepared by recording the absorbance values for a range of known concentrations of dye solutions at the wavelength for maximum absorbance of each dye. The value, λ_{max}, was found from a scan for the dye's spectrum. These values of λ_{max} were used in all subsequent investigations using these dyes. The λ_{max} for Acid Red 114 and Acid Blue 80 are 522 and 626 nm respectively. All measurements were made on a Varian Cary IE spectrophotometer.

Equilibrium Isotherms

Equilibrium studies were carried out to determine the adsorption behaviour for the two dyes onto activated carbon F400. Each system was given a contact time of 21 days to ensure equilibrium had been reached. The isotherms were determined by agitating 0.05 g of activated carbon with 0.05 dm^3 of the dye solution for 21 days at a constant temperature of 20 ± 2°C.

Batch Adsorber Studies

The adsorber vessel used for the contact time experiments was based on the standard mixing tank configuration. A 2 dm^3 plastic beaker of internal diameter 0.13 m was used and contained a volume of 1.7 dm^3 of dye solution. A six-bladed, flat, plastic impeller provided good mixing in the vessel. The diameter of the impeller and the blade height were 0.065 m and 0.013 m respectively. A Heidolph type RZR1 variable-speed motor was used to drive the impeller using a 0.005 m diameter plastic shaft. Six plastic baffles were spaced evenly around the vessel circumference to prevent the formation of a vortex and the consequential reduction in relative motion between liquid and solid particles, and power losses due to air entrainment at the impeller. The polystyrene baffles used were flat strips of 0.2 m long and 0.01 m wide. Kinetic data were collected for a series of system parameters. 3 ml samples were extracted at selected time intervals (up to a maximum of 12 hours) using a 10 ml syringe. The concentration was determined and the results were recorded as concentration versus time decay curves.

Results and Discussion

Sensitivity Analysis

A sensitivity analysis was performed to study the effect of the four model mass-transfer parameters—the external mass transfer coefficient K_f, effective diffusivity

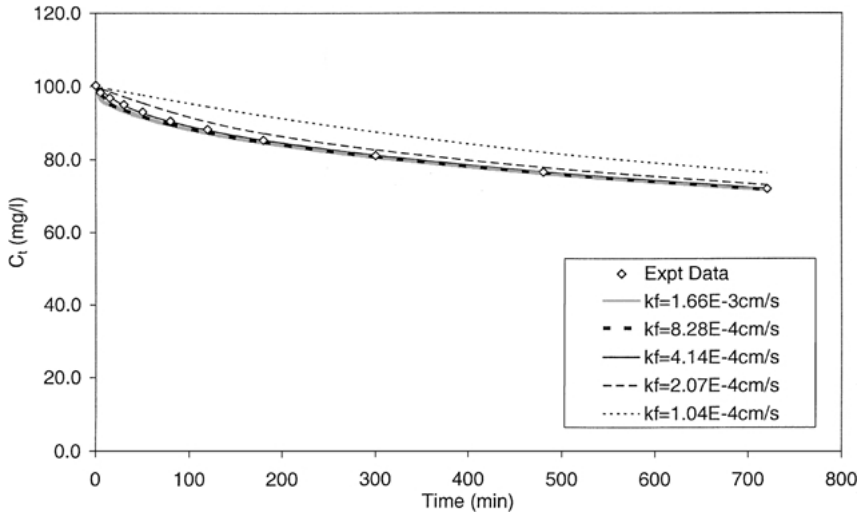

Figure 1. Sensitivity analysis—Effect of external mass transfer coefficient, K_f, on the adsorption of AB80 on activated carbon.

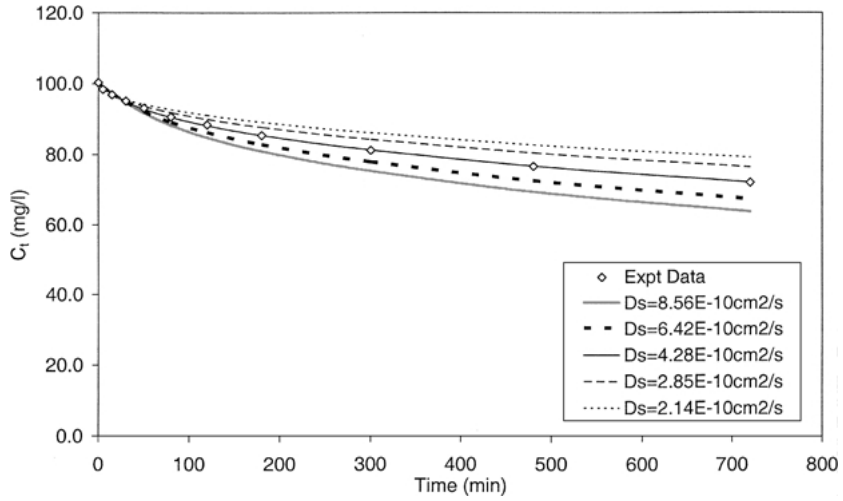

Figure 2. Sensitivity analysis—Effect of diffusion coefficient, D_s, on the adsorption of AB80 on activated carbon.

D_{eff}, lumped micropore diffusion rate parameter K_b and the macropore adsorption capacity factor f—on the shape of the concentration decay curves. The results are shown in Figs. 1–4. In Fig. 1, it can be seen that the external mass transfer coefficient, K_f, predominantly influences the initial gradient of the concentration decay curve and a higher K_f value results in a steeper initial gradient. The effective diffusivity, D_{eff}, affects the adsorption period when macropore diffusion dominates and influences the curvature of the concentration decay curve at the onset of the slow diffusion phase as shown in Fig. 2. A higher D_{eff} value results sharper and more pronounced curvature. Figure 3 shows that the effect of the macropore rate parameter, K_b, becomes evident at later stages where macro- to micropore transport is the dominant feature of adsorption, influencing the slope of the slow diffusion phase. A higher K_b value results in a steeper final slope. The fraction of the total adsorption capacity attributed to macropores, f, determines the position at which the curve departs from the initial gradient and begins the slow sorption phase with a lower f value yielding a lower extent of sorption (over the model time-frame) and a higher solution dye concentration, as illustrated in Fig. 4.

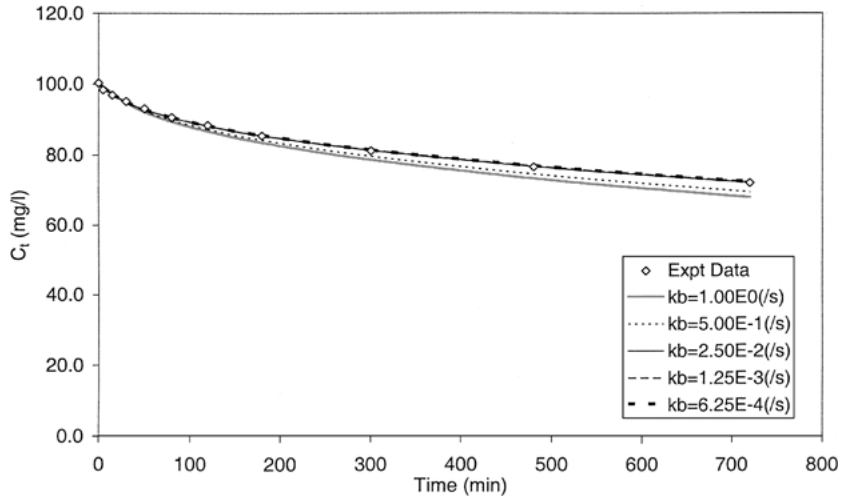

Figure 3. Sensitivity analysis—Effect of micropore rate parameter, K_b, on the adsorption of AB80 on activated carbon.

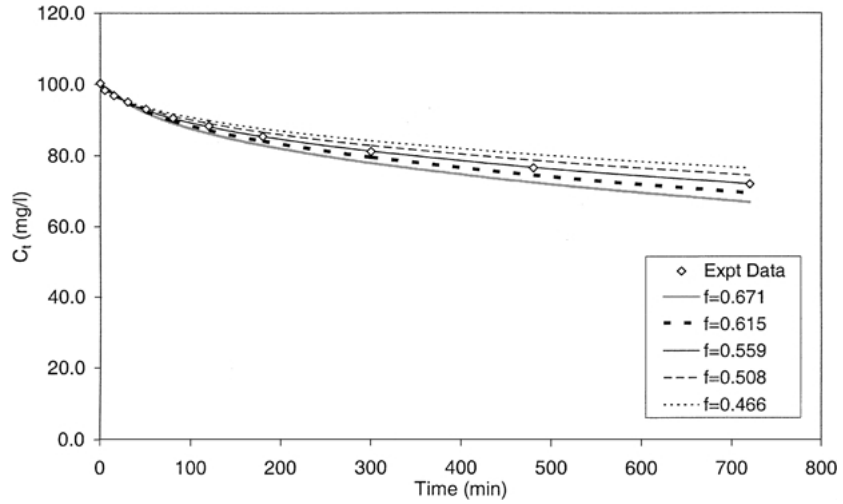

Figure 4. Sensitivity analysis—Effect of fraction of macropore adsorption capacity, f, on the adsorption of AB80 on activated carbon.

Equilibrium Isotherms

The equilibrium surface concentration is an integral part of the Branched Pore Kinetic Model and must be accurately represented to maintain confidence in the accuracy of the model and its results. The equilibrium data were analysed using the Langmuir and Freundlich isotherm:

$$\text{Langmuir isotherm: } q_e = \frac{K_L C_e}{1 + a_L C_e} \tag{53}$$

$$\text{Freundlich isotherm: } q_e = K_F C_e^{1/n} \tag{54}$$

Although the surface of activated carbon F400 is known to be a heterogeneous surface, the Langmuir equation was found to give the best data correlation despite its normal applicability to homogeneous equal energy site adsorption. Consequently the Langmuir form was used although it must be regarded as an empirical form of data correlation. The comparisons of the fitting of the Langmuir and Freundlich isotherms on the experimental equilibrium data for the two dyes are demonstrated in Figs. 5 and 6, and the isotherm constants are presented in Table 1 together with the sum of squares errors (*SSE*) values.

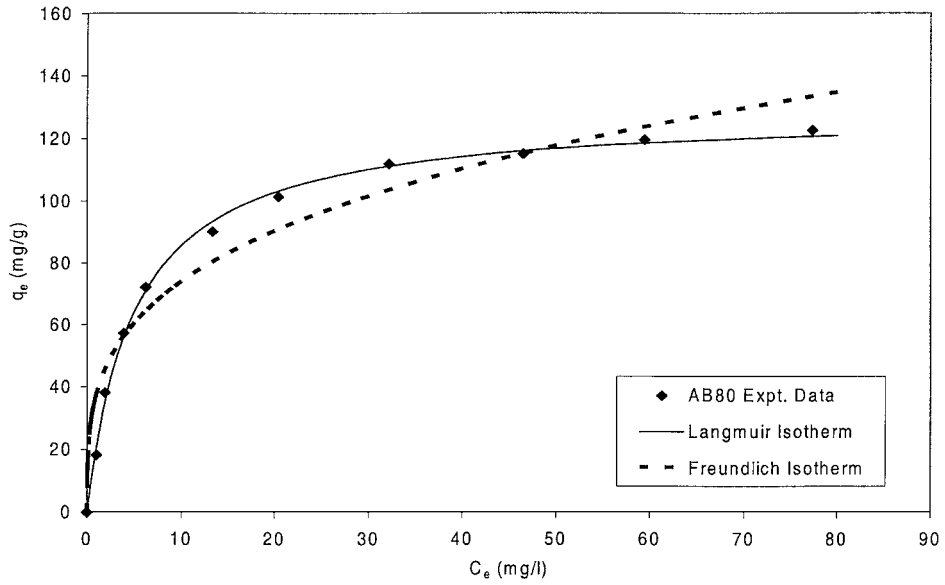

Figure 5. Langmuir and Freundlich adsorption isotherm for Acid Blue 80 on activated carbon.

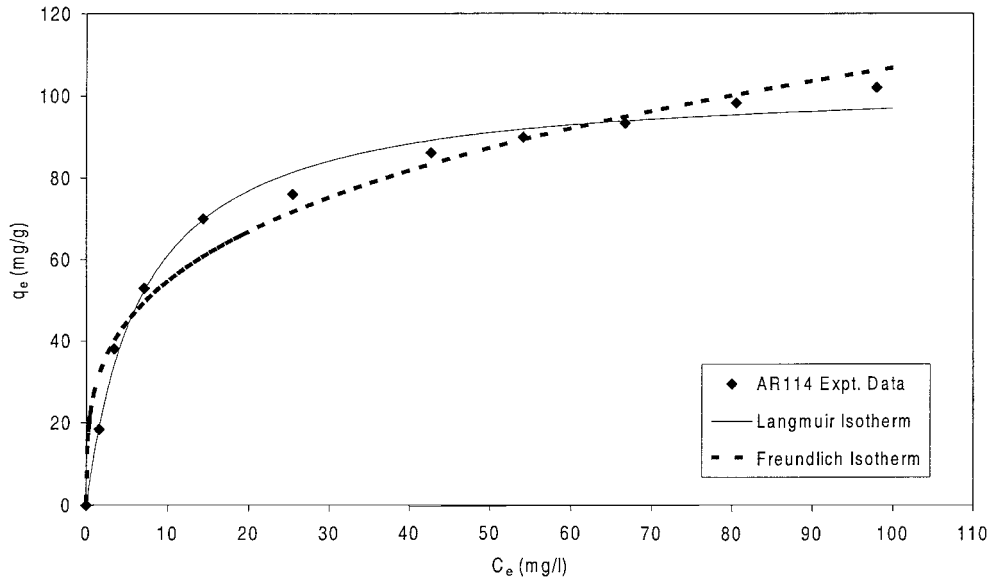

Figure 6. Langmuir and Freundlich adsorption isotherm for Acid Red 114 on activated carbon.

The mechanism of adsorption for acid dyes is connected to the fact that the surface of activated carbon F400 in contact with water is negatively charged. Acid Dyes are examples of dyes which ionize in aqueous solution to form an anionic coloured component D^- and a cation of Na^+. The approach of an acidic dye anion will suffer coulombic repulsion due to the presence of the anionic groups on carbon and therefore the mechanism is predominantly physical adsorption.

Application of the Branched Pore Model

To determine the model parameters for each dye-sorbent system, the model was initially used to determine a set of the four mass-transport parameters

Table 1. Langmuir and Freundlich isotherm constants for the two acid dyes on activated carbon.

	Langmuir isotherm			Freundlich isotherm		
Dye	K_L (dm^3/mg)	a_L (dm^3/mg)	*SSE*	K_F (dm^3/g)	$1/n$	*SSE*
AB80	25.684	0.20	39.2	38.224	0.288	909.0
AR114	14.903	0.14	92.9	28.070	0.290	331.0

Table 2. Constant mass transfer parameters (K_f, D_{eff}, K_b and f) for the adsorption of AB80 on activated carbon.

Mass (g)	C_0 (mg/dm^3)	K_f (cm/s)	D_{eff} (cm^2/s)	K_b (/s)	f (−)	*SSE*
1.7	50	4.20E-04	4.42E-10	2.17E-02	0.5719	36.0
1.7	75					38.6
1.7	100					3.3
1.7	150					111.3
1.7	200					264.9
0.4	100	4.20E-04	4.42E-10	2.17E-02	0.5719	6.1
0.8	100					2.5
1.2	100					1.4
1.7	100					3.3
2.2	100					3.6
Total						467.8

Table 3. Constant mass transfer parameters (K_f, D_{eff}, K_b and f) for the adsorption of AR114 on activated carbon.

Mass (g)	C_0 (mg/dm^3)	K_f (cm/s)	D_{eff} (cm^2/s)	K_b (/s)	f (−)	*SSE*
1.7	50	4.69E-04	4.73E-10	4.09E-03	0.5086	78.2
1.7	75					53.4
1.7	100					15.6
1.7	150					40.9
1.7	200					144.2
0.4	100	4.69E-04	4.73E-10	4.09E-03	0.5086	1.3
0.8	100					5.6
1.2	100					1.7
1.7	100					15.6
2.2	100					15.5
Total						356.3

for each experimental concentration-time decay curve. An average was then taken for each parameter for each of the two dye-sorbent systems. The model was then executed with these average parameter values and the *SSE* values were determined for each set of experimental data. The values of the four parameters for the adsorption of Acid Blue 80 and Acid Red 114 on carbon are shown in Tables 2 and 3. The results are shown in Figs. 7 and 8 for the effect of C_0 and mass for AB80 on carbon respectively. Similarly, Figs. 9 and 10 show the theoretical and experimental results for the effect of C_0 and mass for AR114 respectively. The results show that both sets of data exhibit similar trends in that the errors are greatest at lowest and highest C_0 for both dye systems, suggesting that D_{eff} may vary with the initial dye concentration.

Since it has previously been established that surface diffusivity can vary with liquid concentration and surface loadings (Gilliland et al., 1974; Muraki et al., 1982; Suzuki and Fujii, 1982; Miyahara and Okazaki, 1992;

Table 4. Variable D_{eff} optimisation results for the adsorption of AB80 on activated carbon.

Mass (g)	C_0 (mg/dm^3)	K_f (cm/s)	D_{eff} (cm^2/s)	K_b (/s)	f (−)	*SSE*
1.7	50	4.20E-04	2.61E-10	2.17E-02	0.5719	1.5
1.7	75		3.02E-10			1.2
1.7	100		4.07E-10			0.8
1.7	150		6.94E-10			3.6
1.7	200		8.49E-10			2.1
0.4	100	4.20E-04	2.55E-10	2.17E-02	0.5719	0.5
0.8	100		3.77E-10			0.5
1.2	100		4.15E-10			0.6
1.7	100		4.07E-10			0.8
2.2	100		4.17E-10			1.5
Total						12.3

Table 5. Variable D_{eff} optimisation results for the adsorption of AR114 on activated carbon.

Mass (g)	C_0 (mg/dm^3)	K_f (cm/s)	D_{eff} (cm^2/s)	K_b (/s)	f (−)	*SSE*
1.7	50	4.69E-04	1.85E-10	4.09E-03	0.5086	3.2
1.7	75		2.79E-10			1.1
1.7	100		3.66E-10			1.7
1.7	150		6.75E-10			3.2
1.7	200		8.89E-10			2.5
0.4	100	4.69E-04	4.82E-10	4.09E-03	0.5086	1.3
0.8	100		5.21E-10			5.0
1.2	100		4.69E-10			1.7
1.7	100		3.66E-10			1.7
2.2	100		3.88E-10			1.9
Total						21.5

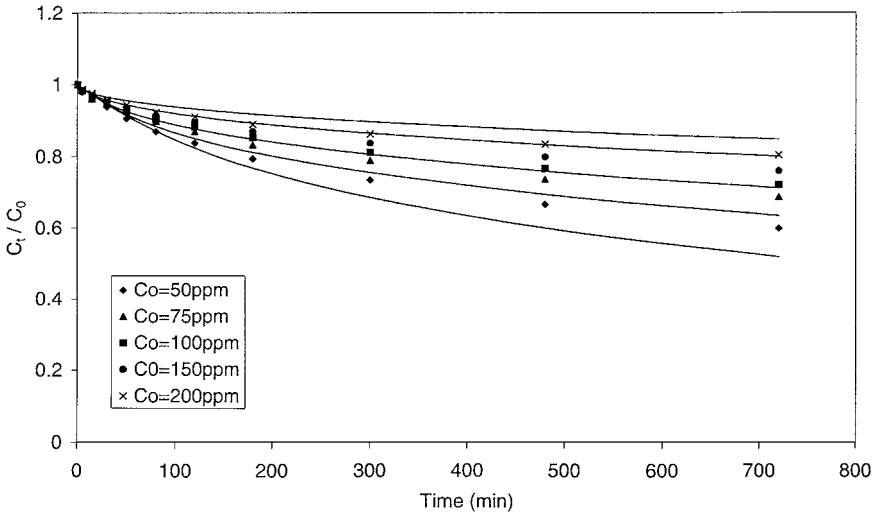

Figure 7. Effect of initial dye concentration on the adsorption of Acid Blue 80 on activated carbon ($m = 1.7$ g) with constant K_f, D_{eff}, K_b and f.

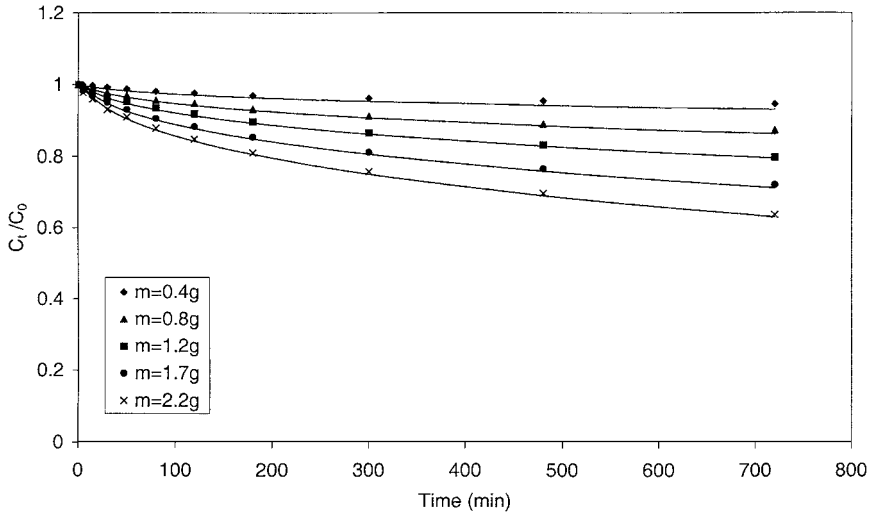

Figure 8. Effect of carbon mass on the adsorption of Acid Blue 80 on activated carbon ($C_0 = 100$ ppm) with constant K_f, D_{eff}, K_b and f.

Min et al., 1998, Do, 1998), in the second application of the model only three of the mass-transport parameters were fixed (K_b, K_f and f) while D_{eff} was retained as a variable. Figures 11 and 12 show the influence of varying D_{eff} on the adsorption of AB80 on carbon and Figs. 13 and 14 show the concentration-time decay curves for AR114 using a variable D_{eff}. The best-fit parameters and *SSE* values under these conditions are presented in Tables 4 and 5 for the adsorption of AB80 and AR114 onto activated carbon respectively.

Comparing the *SSE* values in Table 5 with those in Table 3, all the *SSE* values in Table 5 are very low. This quality is reflected in the visual agreement between experimental and theoretical concentration decay cuves shown in Figs. 13 and 14. Good agreement is observed for all ranges of carbon masses and initial dye concentration examined. For AR114 the use of a variable D_{eff} results in a significant improvement of the fit, with the *SSE* value decreases from 356.3 to 21.5. The largest improvements were observed for decay curves measured at high initial dye concentrations.

For determining the average D_{eff} for the sorption of AB80 on activated carbon the value was based on the experiments using $C_0 = 50, 75, 100, 150$ and

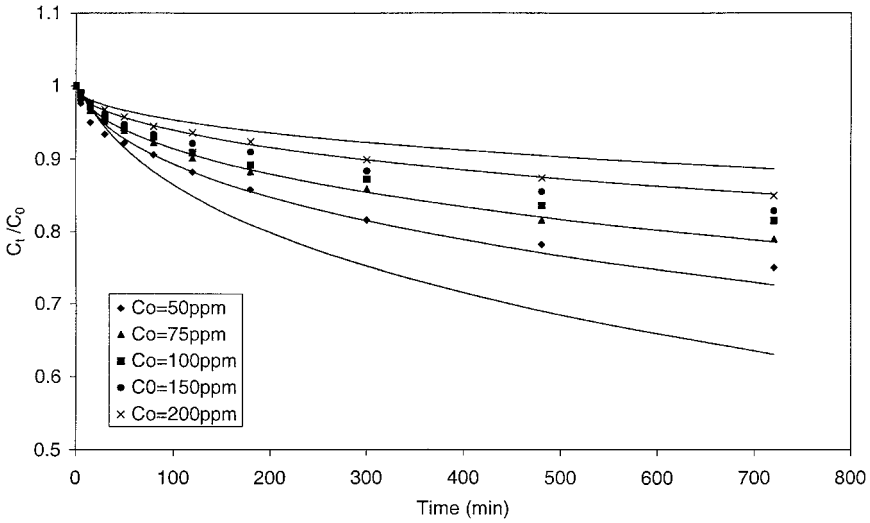

Figure 9. Effect of initial dye concentration on the adsorption of Acid Red 114 on activated carbon ($m = 1.7$ g) with constant K_f, D_{eff}, K_b and f.

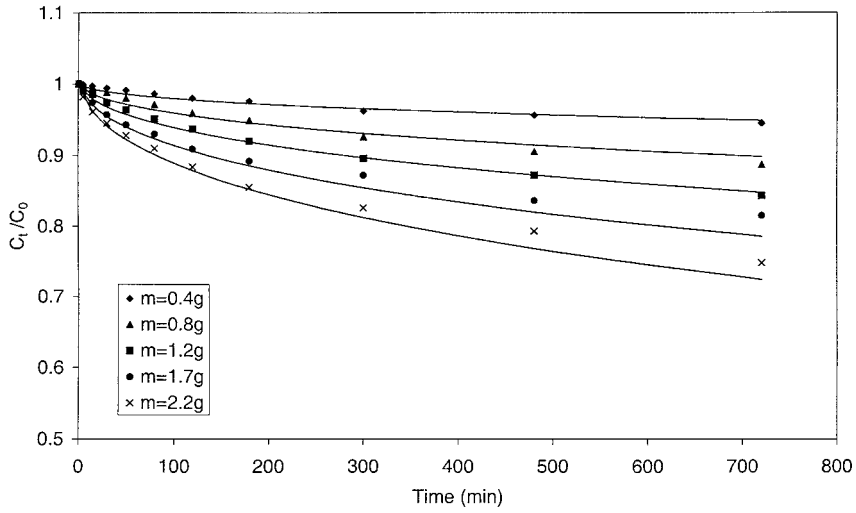

Figure 10. Effect of carbon mass on the adsorption of Acid Red 114 on activated carbon ($C_0 = 100$ ppm) with constant K_f, D_{eff}, K_b and f.

200 mg · dm^{-3} and carbon mass = 0.4, 0.8, 1.2, 1.7 and 2.2 g. The *SSE* values and the parameters for the AB80 data are listed in Table 2 using the single fixed D_{eff} value and in Table 4 for a variable D_{eff} and plots comparing the theoretical data with the experimental values are shown in Figs. 11 and 12. The data for AB80 exhibit similar trends to those observed for AR114—for both carbon mass and initial dye concentration the model correlation with the experimental data is improved significantly by the use of variable D_{eff}. The largest improvements were again observed for concentration decay curves measured at high initial dye concentration.

Previous attempts to account for variable surface diffusivities have examined the dependence on fractional surface coverage, λ, which is the same form as the Darken equation for the Langmuir isotherm (Darken, 1948; Do, 1998):

$$D_{\text{eff}} = \frac{D_{\text{eff},\infty}}{1 - \lambda} \tag{55}$$

This form did not correlate the D_{eff} value in the present solution, again suggesting the heterogeneous nature of the carbon surface even though the equilibrium data could be correlated by a Langmuir type equation.

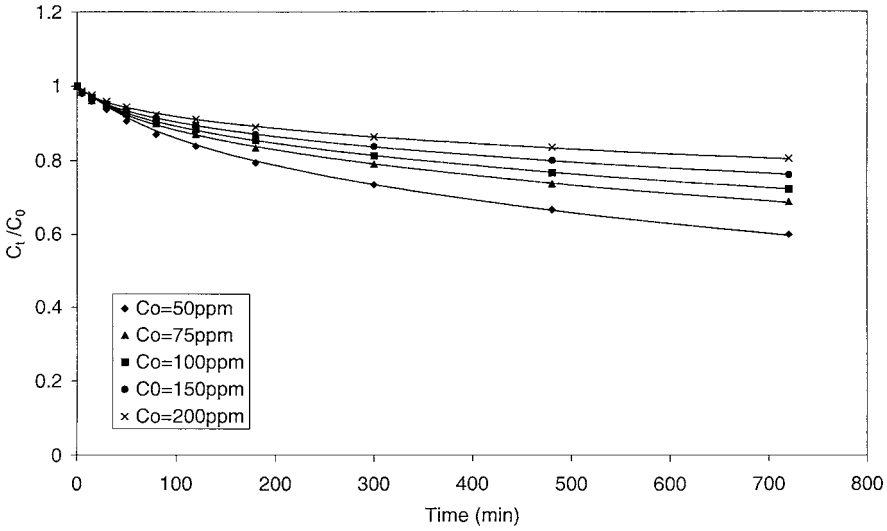

Figure 11. Effect of initial dye concentration on the adsorption of Acid Blue 80 on activated carbon ($m = 1.7$ g) with variable D_{eff} and constant K_f, K_b and f.

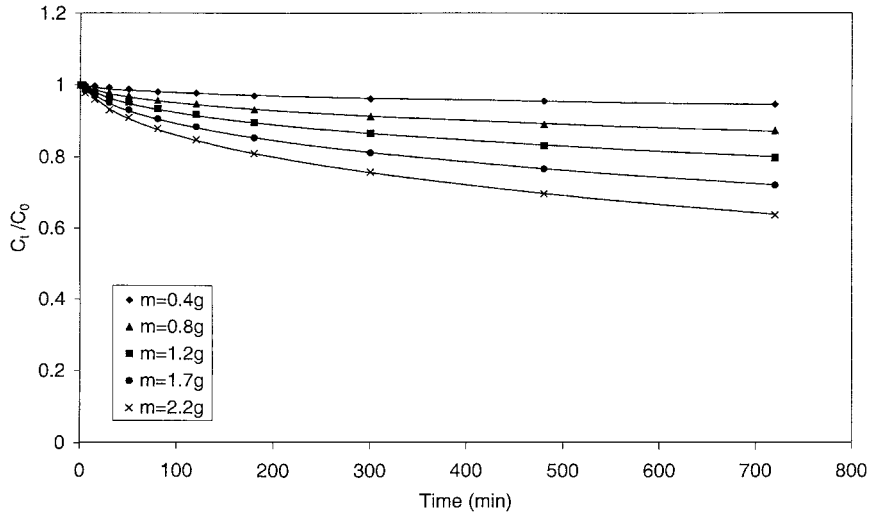

Figure 12. Effect of carbon mass on the adsorption of Acid Blue 80 on activated carbon ($C_0 = 100$ ppm) with variable D_{eff} and constant K_f, K_b and f.

Suzuki and Fujii (1982) demonstrated that the strong dependence of surface diffusion coefficient on the amount adsorbed q could be interpreted in terms of the change of heat of adsorption with surface coverage:

$$D_s = D_{s0}(\kappa \cdot q)^n \tag{56}$$

where n is the exponent in the Freundlich isotherm.

However, using the Freundlich exponent based equation still did not enable D_s to be correlated with surface coverge. This indicates that D_{eff} may be a complex function dependent on both the isotherm and an adsorbed species concentration/mobility expression.

By considering a general form of Eq. (56), the effective diffusivities as surface diffusivities may be correlated by the following expression:

$$D_{\text{eff}} = D_{\text{eff},\infty}(\bar{q}/q_0)^{\gamma} \tag{57}$$

where $\bar{q}$ is the averaged solid phase concentration for each set of experimental data; q_0 is the saturated solid phase concentration in equilibrium with C_0.

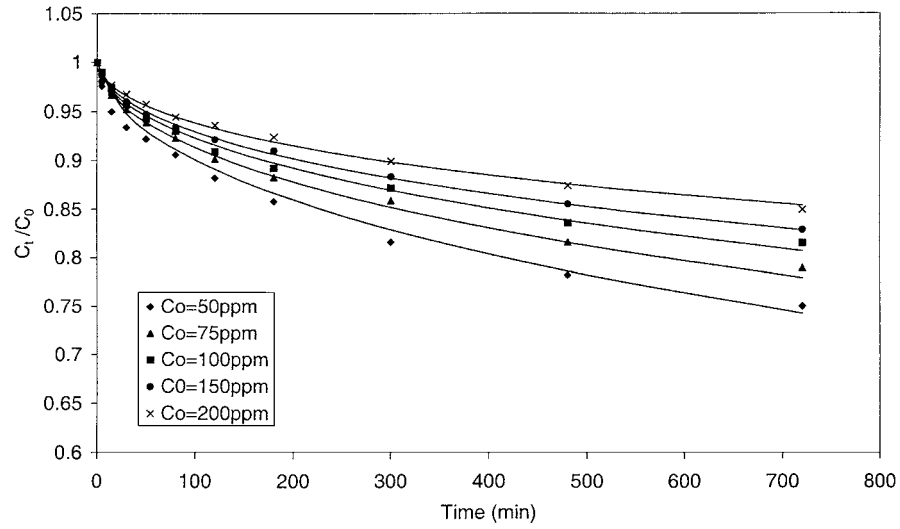

Figure 13. Effect of initial dye concentration on the adsorption of Acid Red 114 on activated carbon ($m = 1.7$ g) with variable D_{eff} and constant K_f, K_b and f.

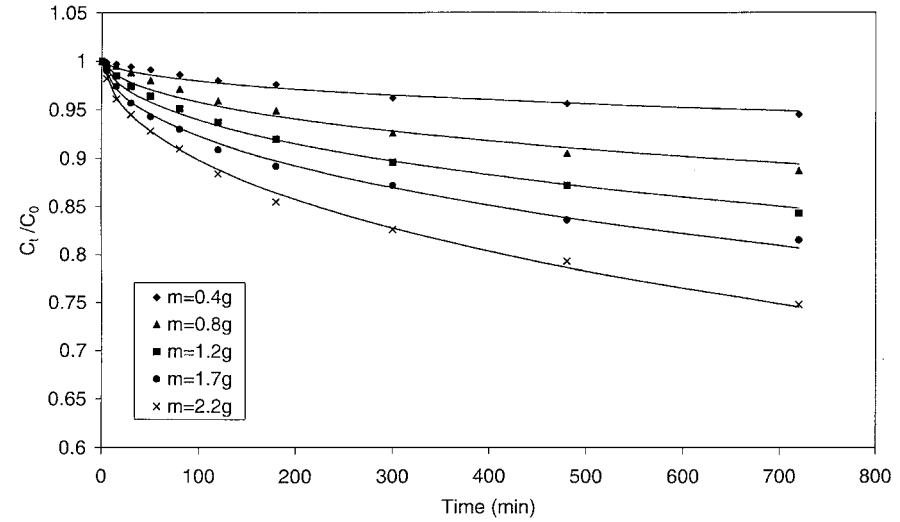

Figure 14. Effect of carbon mass on the adsorption of Acid Red 114 on activated carbon ($C_0 = 100$ ppm) with variable D_{eff} and constant K_f, K_b and f.

Figures 15 and 16 shows plots of D_{eff} against $\bar{q}/q_0$ for the two dye-carbon systems, and the expressions for the two dyes are:

$$\text{AB80}: \quad D_{\text{eff}} = 1.98 \times 10^{-8} \times (\bar{q}/q_0)^{2.07} \quad (58)$$

$$\text{AR114}: \quad D_{\text{eff}} = 2.90 \times 10^{-8} \times (\bar{q}/q_0)^{2.16} \quad (59)$$

The exponents based on the best fit Freundlich equation for AB80 and AR114 are 3.47 and 3.45 respectively; the best fit exponents, namely, 2.07 and 2.16 reflect the poorness of fit of the Freundlich equation. The correlation coefficients for the Eqs. (58) and (59) are 0.9922 and 0.9994 respectively. The deviation from linearity of Figs. 15 and 16 may be due to the fact that the points are not individual D_{eff} values for individual experimental data points, but rather averaged D_{eff} values for final $\bar{q}/q_0$ values for experimental systems not individual points.

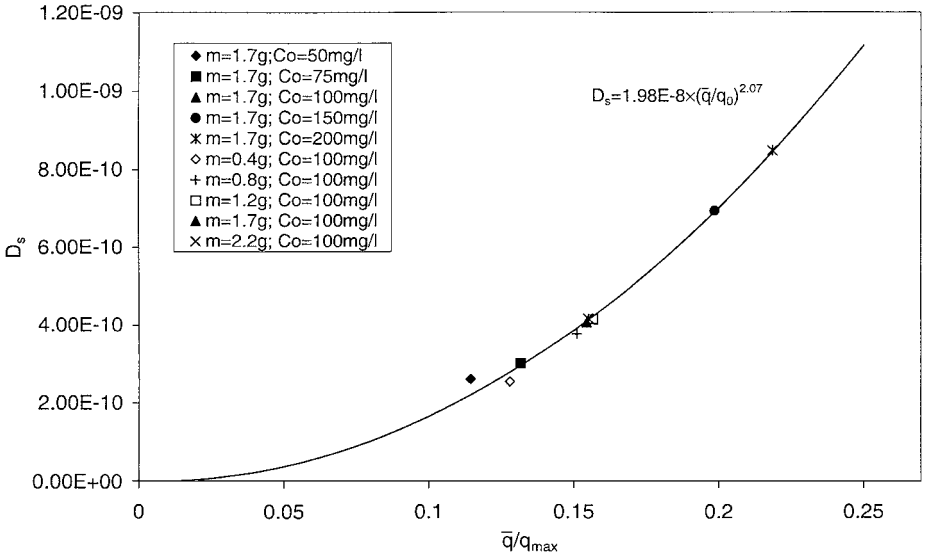

Figure 15. Relationship between the optimised diffusion coefficients with a function of surface coverage for AB80 on activated carbon.

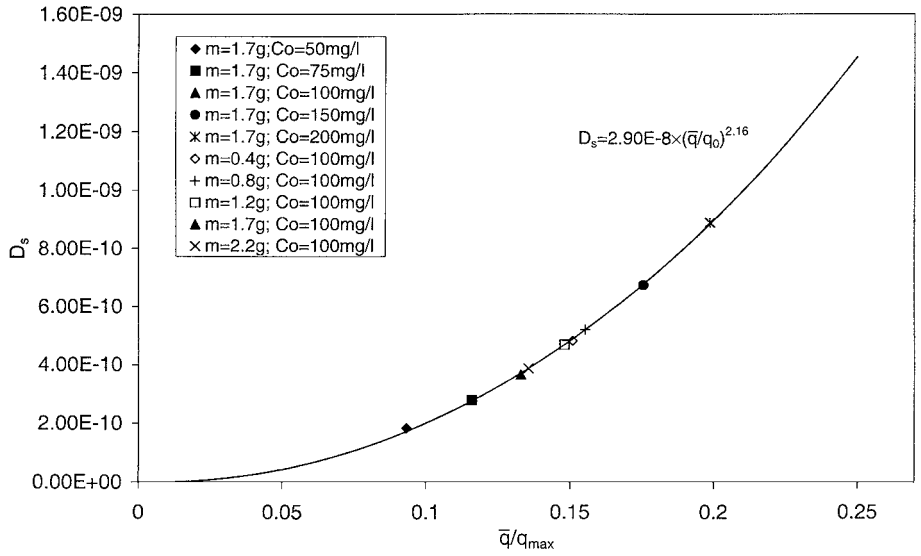

Figure 16. Relationship between the optimised diffusion coefficients with a function of surface coverage for AR114 on activated carbon.

Conclusions

From the present work the following points can be made.

1. The branched-pore model has been shown to be applicable over a wide range of experimental conditions for the adsorption of the two acid dyes AB80 and AR114 on activated carbon.
2. Single values for the diffusion parameters K_f, D_{eff}, K_b and f can be used to predict the concentration versus time decay curves over much of the range of masses and concentrations of each dye system, with reasonable accuracy.
3. A significantly better fit of the model predictions is obtained when K_f, K_b and f are maintained constant but D_{eff} is varied. This indicates that the surface diffusivity may vary as a function

of either the liquid or solid phase concentrations.

4. The effective diffusion coefficients obtained by minimization of the *SSE* value can be correlated with a reasonable degree of accuracy by a function of surface coverage.

Nomenclature

A	Total surface area of particles (cm^2)
a_L	Langmuir isotherm constants ($dm^3\ mg^{-1}$)
C_e	Equilibrium fluid-phase concentration ($mg\ dm^{-3}$)
C_0	Initial liquid phase solute concentration ($mg\ dm^{-3}$)
$C_{s,t}$	Liquid phase concentration at particle surface at time t ($mg\ dm^{-3}$)
C_t	Liquid phase concentration at time t ($mg\ dm^{-3}$)
d_p	Diameter of the particle (cm)
D_{eff}	Effective diffusivity ($cm^2\ s^{-1}$)
D_s	Surface diffusion coefficient ($cm^2\ s^{-1}$)
f	Fraction of total adsorptive capacity in macropores (dimensionless)
k	Intraparticle mass transfer coefficient ($cm\ s^{-1}$)
K_b	Branched pore rate coefficient (s^{-1})
K_f	External liquid film mass transfer coefficient ($cm\ s^{-1}$)
K_F	Freundlich isotherm constants ($dm^3\ g^{-1}$)
K_L	Langmuir isotherm constants ($dm^3\ g^{-1}$)
m	Mass of adsorbent (g)
n	Freundlich isotherm constants (dimensionless)
q_b	Solid phase concentration in micropore region ($mg\ g^{-1}$)
q_e	Equilibrium solid phase concentration ($mg\ g^{-1}$)
q_m	Solid phase concentration in macropore region ($mg\ g^{-1}$)
q_0	Solid phase concentration in equilibrium with C_0 ($mg\ g^{-1}$)
q_s	Solid phase concentration at particle surface ($mg\ g^{-1}$)
r	Radial distance from centre of particle (cm)
R	Radius of particle (cm)
R_b	Rate of transfer of solute from macropore to micropore region ($mg\ g^{-1}\ s^{-1}$)
SSE	Sum of squares errors $= \sum_{i=1}^{n}(C_{\text{Experimental},i} - C_{\text{Theoretical},i})^2$
t	Time (s)
Vol	Volume of batch solution (dm^3)
V	Volume of particles (cm^3)
C	Dimensionless liquid phase concentration ($= \frac{C_t}{C_0}$)
C_n	Value of C at nth grid point of θ mesh
C_s	Dimensionless liquid phase concentration at particle surface ($= \frac{C_{s,t}}{C_0}$)
Q_m	Dimensionless solid phase concentration in macropore region ($= \frac{q_m}{q_0}$)
Q_b	Dimensionless solid phase concentration in micropore region ($= \frac{q_b}{q_0}$)
Q_s	Dimensionless solid phase concentration at particle surface
$PBiot$	Modified particle Biot number ($= \frac{K_b R^2}{f D_{\text{eff}}}$)
$FBiot$	Modified film Biot number ($= \frac{K_f C_0 R^2}{\rho f D_{\text{eff}} q_0}$)
$SFact$	Separation factor ($= \frac{V C_0}{m q_0}$)
M	Last grid point of η mesh corresponding to particle surface
Q_p^n	Value of Q_m at pth mesh point of η grid and nth mesh point of θ grid
$\bar{Q}_p^n$	Value of Q_b at pth mesh point of η grid and nth mesh point of θ grid
S_1	$\frac{\Delta\theta}{\Delta\eta}$
S_2	$\frac{(PBiot) f \Delta\theta}{2(1-f)}$
S_3	$\frac{3 f (FBiot) \Delta\theta}{2(SFact)}$
S_4	$\frac{\Delta\eta (FBiot)}{2}$

Greek Letters

κ	Constant defined in Eq. (56) ($g\ mg^{-1}$)
λ	Surface coverage ($= \frac{q}{q_0}$)
β	Reduced radial variable ($= \frac{r}{R}$)
ρ	Adsorbent particle density ($g\ cm^{-3}$)
θ	Dimensionless time variable ($= \frac{D_{\text{eff}} t}{R^2}$)
$\Delta\theta$	Spacing of finite difference mesh in variable θ
η	Transformed radial variable ($= \beta^2$)
$\Delta\eta$	Spacing of finite difference mesh in variable η

References

Allen, S.J., P. Brown, G. McKay, and O. Flynn, "An Evaluation of Single Resistance Transfers Models in the Sorption of Metal Ions by Peat," *J. Chem. Technol. Biotechnol.*, **54**, 271–276 (1992).

Crank, J. and P. Nicolson, "A Practical Method for Numerical Evaluation of Solutions of Partial Differential Equations of the Heat-Conduction Type," *Math. Proceedings of the Cambridge Philosophical Society*, **43**, 50–67 (1947).

Crittenden, J.C. and W.J. Weber, Jr., "Predictive Model for Design of Fixed-Bed Adsorbers: Parameter Estimation and Model Development," *ASCE J. Env. Eng. Div.*, **104**(2), 185–197 (1978a).

Crittenden, J.C. and W.J. Weber, Jr., "Predictive Model for Design of Fixed-Bed Adsorbers: Single-Component Model Verification," *ASCE J. Env. Eng. Div.*, **104**(3), 433–443 (1978b).

Darken, L.S., "Diffusion, Mobility and their Interrelation through Free Energy in Binary Metallic Systems," *Trans. of Amer. Inst. of Min. Eng.*, **175**, 184–201 (1948).

Dedrick, R.L. and R.B. Beckmann, "Pore and Solid Diffusion Models for Batch Adsorbers," *Chem. Eng. Progr. Symp. Ser.*, **63**(74), 68–81 (1967).

DiGiano, F.A. and W.J. Weber, Jr., "Sorption Kinetics in Finite-Bath Systems," *ASCE J. Env. Eng. Div.*, **98**(SA6), 1021–1036 (1972).

Do, D.D. *Adsorption Analysis: Equilibria and Kinetics*, Imperial College Press, London, 1998.

Edeskuty, F.J. and N.R. Amundson, "Effects of Intraparticle Diffusion in Agitated Static Systems," *Ind. Eng. Chem.*, **44**, 1968 (1952).

Famularo, J., J.A. Mueller, and A.S. Pannu, "Prediction of Carbon Column Performance from Pure Solute Data," *J. Wat. Poll. Contr. Fed.*, **52**(7), 2019–2032 (1980).

Gilliland, E., R.F. Baddour, G.P. Perkinson, and K.J. Sladek, "Diffusion on Surfaces. I. Effect of Concentration on the Diffusivity of Physically Adsorbed Gases," *Ind. Eng. Chem. Fundam.*, **13**(2), 95–100 (1974).

Glueckauf, E., "Formulas for Diffusion in Spheres and their Applications," *Trans. Faraday Soc.*, **51**, 1540–1552 (1955).

Griffin, R.P. and J.S. Dranoff, "Rate of Glycerol Adsorption by Ion Exchange Resins," *AIChE J.*, **9**, 283–291 (1963).

Hsieh, J.S., R.M. Turian, and C. Tien, "Experimental Investigation of the Adsorption of Organic Contaminants in Waste Water on Granular Activated Carbon," Research Report Number RR-69-1, *Fed. Water Poll. Control Admin.*, U.S. Department of Interior, 1969.

Hu, X., "Multicomponent Adsorption Equilibrium of Gases in Zeolites: Effect of Pore Size Distribution," *Chem. Eng. Comm.*, **174**, 201–214 (1999).

Hu, X., S. Qiao, and D.D. Do, "Multicomponent Adsorption Kinetics of Gases in Activated Carbon: Effect of Pore Size Distribution," *Langmuir*, **15**, 6428–6437 (1999).

Jury, S.H., "Improved Version of the Rate Equation for Molecular Diffusion in a Dispersed Phase," *AIChE J.*, **13**, 1124–1135 (1967).

Kasten, P.R. and N.R. Amundson, "Effect of Intraparticle Diffusion: Analytical Solution for Simple Systems in Moving-Bed Adsorbes," *Ind. Eng. Chem.*, **44**(7), 1704–1715 (1952).

Keinath, T.M. and W.J. Weber, Jr., Tech. Pub., Res. Proj. No. W.P. 00706, *Fed. Water Poll. Control Admin.*, U.S. Department of Interior, 1968.

Lee, M.C., W.E. Thacker, V.L. Snoeyink, and J.C. Crittenden, "Mathematical Modeling of Humic Substances Removal with Activated Carbon Beds," *ASCE Environmental Engineering Conference Proceedings*, pp. 387–393 (1980).

Mathews, A.P. and W.J. Weber, Jr., "Effects of External Mass Transfer and Intraparticle Diffusion on Adsorption Rates in Slurry Reactors," *AIChE Symp. Ser.*, **73**, 166 (1976).

McKay, G., "Analytical Solution Using a Pore Diffusion Model for a Pseudo Irreversible Isotherm for the Adsorption of Basic Dye on Silica," *AIChE J.*, **30**(4), 692–697 (1984a).

McKay, G., "The Adsorption of Basic Dye onto Silica from Aqueous Solutions-Solid Diffusion Model," *Chem. Eng. Sci.*, **39**, 129–138 (1984b).

McKay, G., S. McKee, and H.R.J. Walters, "Solid-Liquid Adsorption Based on External Mass Transfer, Macropore and Micropore Diffusion," *Chem. Eng. Sci.*, **42**(5), 1145–1151 (1987).

Min, Y.H, K.S. Lee, C.S. Yoon, and L.M. Do, "Surface Morphology Study of Corona-Poled Thin Films Derived from Sol-Gel Processed Organic-Inorganic Hybrid Materials for Photonics Applications," *J. Materials Chem.*, **8**(5), 1225–1232 (1998).

Miyahara, M. and M. Okazaki, "Concentration Dependence of Surface Diffusivity of Nitrobenzene and Benzonitrile in Liquid Phase Adsorption onto an Activated Carbon," *J. Chem. Eng. Japan*, **25**, 408–414 (1992).

Muraki, M., Y. Iwashima, and T. Hayakawa, "Rate of Liquid-Phase Adsorption on Activated Carbon in the Stirred Tank," *J. Chem. Eng. Japan*, **15**(1), 34–39 (1982).

NAG, *The NAG Fortran Library Introductory Guide*, Mark 16, The Numerical Algorithms Group Ltd., 1993.

Neretnieks, I., "Analysis of Some Adsorption Experiments with Activated Carbon," *Chem. Eng. Sci.*, **31**(11), 1029–1035 (1976).

Peel, R.G., A. Benedek, and C.M. Crowe, "A Branched Pore Kinetic Model for Activated Carbon Adsorption," *AIChE J.*, **27**(1), 26–31 (1981).

Spahn, H. and E.U. Schlunder, "Scale-up of Activated Carbon Columns for Water Purification, Based on Results from Batch Tests: 1. Theoretical and Experimental Determination of Adsorption Rates of Single Organic Solutes in Batch Tests," *Chem. Eng. Sci.*, **30**, 529–537 (1975).

Suzuki, M. and T. Fujii, "Concentration Dependence of Surface Diffusion Coefficient of Propionic Acid in Activated Carbon Particles," *AIChE J.*, **28**(3), 380–385 (1982).

Thacker, W.E., V.L. Snoeyink, and J.C. Crittenden, "Modeling of Activated Carbon and Coal Gasification Char Adsorbents in Single Solute and Bi-Solute Systems," University of Illinois, Urbana-Champaign, Water Resources Center, Research Report 0 (161), pp. 1–166, 1981.

Tien, C., *Adsorption Calculations and Modelling*, Butterworth-Heinemann, Newton MA, 1994.

Weber, T.W. and R.K. Chakravorti, "Pore and Solid Diffusion Models for Fixed-Bed Adsorbers," *AIChE J.*, **20**(2), 228–238 (1974).

Weber, W.J., Jr. and S. Liang, "Dual Particle-Diffusion Model for Porous Adsorbents in Fixed Beds," *Env. Progr.*, **2**(3), 167–175 (1983).

Weber, W.J., Jr. and K.T. Liu, "Determination of Mass Transport Parameters for Fixed-Bed Adsorbers," *Chem. Eng. Comm.*, **6**, 49–60 (1980).

Wild, K.A., *Multicomponent Adsorption Column Parameter Studies in Activated Carbon Adsorption*, Vol. I, I.H. Suffet and M.J. McGuire (Eds.), p. 251, Ann Arbor Science Publishers, Ann Arbor MI, 1980.

Yang, X.Y. and B. Al-Duri, "Application of Branched Pore Diffusion Model in the Adsorption of Reactive Dyes on Activated Carbon," *Chem. Eng. J.*, **83**, 15–23 (2001).

Yiacoumi, S. and C. Tien, *Kinetics of Metal Ion Adsorption from Aqueous Solutions*, Kluwer Academic, Boston MA, 1995.